RSC Advances

ROYAL SOCIETY OF CHEMISTRY

www.rsc.org/advances

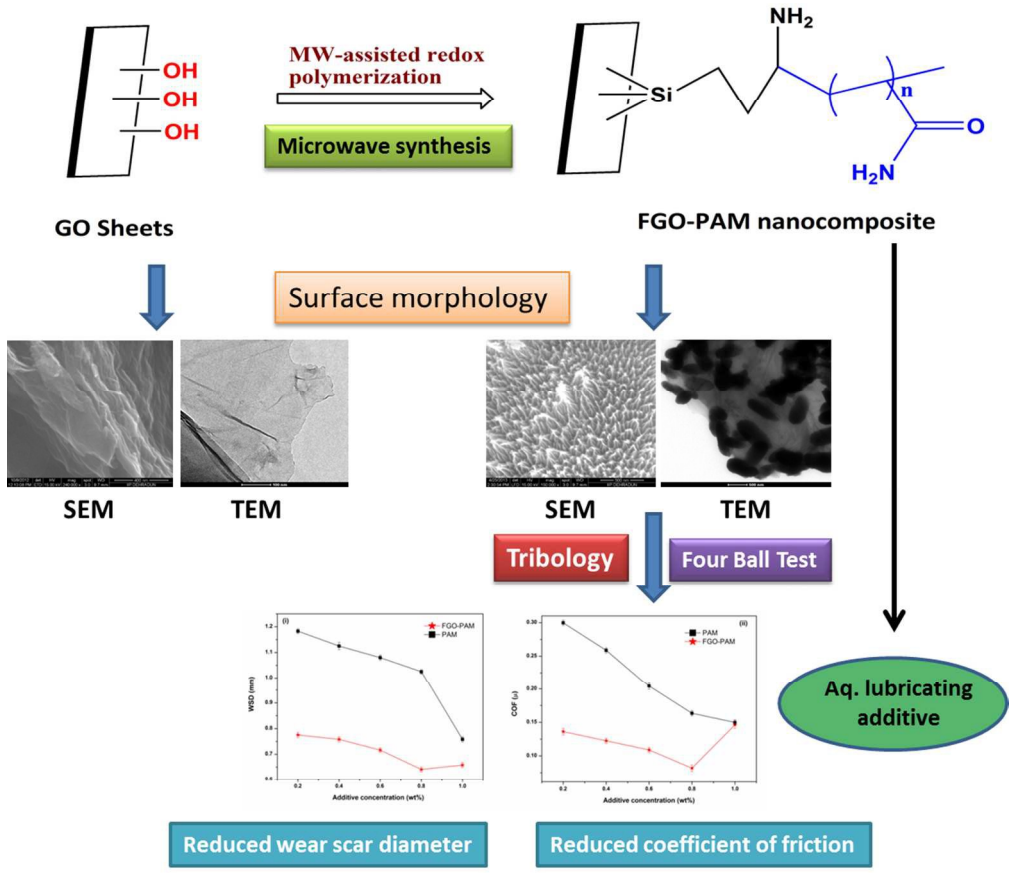

A fast, efficient and greener synthesized FGO-PAM nanocomposite as an improved aqueous lubricating additive
315x274mm (96 x 96 DPI)

Cite this: DOI: 10.1039/c0xx00000x

www.rsc.org/xxxxxx

ARTICLE TYPE

Microwave-assisted surface-initiated redox polymerization of acrylamide with functionalized graphene oxide for aqueous lubricant additive

Arvind Kumar, Babita Behera and Siddharth S. Ray*

Received (in XXX, XXX) Xth XXXXXXXXX 20XX, Accepted Xth XXXXXXXXX 20XX
DOI: 10.1039/b000000x

Abstract A fast and much efficient approach for the synthesis of nanocomposites of polyacrylamide-grafted-functionalized graphene oxide (FGO-PAM) through microwave-assisted surface initiated-redox polymerization (SI-RP) of acrylamide using functionalized graphene oxide and Ce (IV) ions as redox couple in aqueous medium. The nanocomposites are characterized by FT-IR, UV-Vis, Raman, XRD, TGA, FE-SEM, and HRTEM. These characterizations indicate a facile synthesis of macromolecular brushes of polyacrylamide on the surface of graphene oxide. The high dispersion ability and composition ratio of the components facilitate to explore and evaluate the lubrication characteristic of this composite as an additive in aqueous medium. The results showed a substantial reduction of friction coefficient (46-55%) and improvement in anti-wear properties (13-37%), due to formation of lubricating nanolayers of the nanocomposite between the two frictional surfaces, thus qualifying this nanocomposite as an aqueous lubricating additive for tribological application.

Introduction

Graphene oxide (GO) has been emerged as a novel nanomaterial in the field of nano-material science having promising applications in nanocomposites,[1-4] catalytic activity,[5] nanoelectronic[6] and biomedicines[7]. GO is a solution-dispersible, dominantly two dimensional sp^2 carbon sheets and intermediate for the synthesis of graphene. GO is generally obtained from various forms of graphite, most commonly from graphite flakes by chemical oxidation followed by exfoliation[8]. During GO synthesis, the strong oxidation results many oxygenated groups such as hydroxyl, carboxyl and epoxy groups, thus the process not only improves the solubility of GO but also sets targets for further chemical functionalization.[3] These oxy functional groups of GO can be used as sites for polymerization by means of "grafting to" and "grafting from" approaches. In most of cases, "grafting to" method requires hydroxyl or amino groups containing polymers for covalent bonding to graphene oxide through esterification or amidation reactions.[9,10] Kan et al.[4] reported for GO based two dimensional molecular brushes synthesized by free radical polymerization. Wu et al.[11] introduced click chemistry for grafting of polystyrene to GO sheets.

In contrast, "grafting from" approach involves the polymerization initiated on the surface of GO sheets. By this technique polymer composite is produced on surface of GO with high grafting density.[12] Grafting of polymer on GO by various methods such as atom transfer radical polymerization (ATRP),[13,14] reversible addition-fragmentation chain transfer polymerization (RAFT),[15] and single-electron-transfer living radical polymerization (SET-LRP)[16] using various vinyl monomers are reported. Recently, we reported a novel visible light induced SI-ATRP method for grafting of polymethyl methacrylate on titania/reduced graphene oxide nanocomposite.[17] These methods employ surface-initiated controlled radical polymerization (SI-CRP), in which the hydroxyl or carboxylic groups on GO are modified by alkyl halides to generate initiators for polymerization. However, all of the above mentioned methods involve multi-step chemical treatment with large amount of organic solvents. Therefore, it is challenging to explore a facile, environment friendly initiator platform that can be used in aqueous medium for SI-CRP.

Redox reaction systems of Ce (IV) ions with reducing agents such as amines, alcohols, aldehydes, ketones, thiols etc. in aqueous medium forming redox couples are used as initiator for vinyl polymerization.[18] Ce (IV) ions introduce active sites to reductant by a single electron-transfer process thus creating initiation sites. The possibility of homo-polymer formation is reduced due to availability of initiation sites are only on GO surface. Ce (IV) ions initiated grafting polymerization has been successfully employed to prepare polymer brushes on flat substrates.[19-21] Wang et al.[19] prepared poly(N-isopropylacrlamide) on 3-aminopropyltriethoxysilane (APTES) functionalized glass surface through surface initiated–redox polymerization (SI-RP) technique. Pie et al.[20] reported the preparation of water soluble CNT-g-polyacrylamide nanocomposites via SI-RP using redox reaction of ceric ions with amino groups on MWCNTs. Recently, synthesis of polymer grafted GO sheets using Ce (IV) redox system in an aqueous medium with different vinyl monomers are reported.[21,22] Therefore, there is a great scope in Ce (IV) initiated grafting polymerization with functionalized GO sheets, which can

lead to a higher grafting density with an advantage of controlling the polymer chains on two dimensional carbon sheets. Moreover, GO being derivative of graphite sheets, thus inherits the tribological properties like low friction and anti wear form its parental precursor.[23, 24] GO/polyimide[25] and GO/nitrile rubber[26] nanocomposites have been investigated for their tribological properties.

In this paper, we have successfully prepared FGO-PAM nanocomposite using APTES functionalized GO and Ce (IV) ions as a redox system, acrylamide as monomer under microwave polymerization. The microwave-assisted synthesis are usually much faster and more efficient than conventional polymerization methods.[27] The method involves initial formation of stable silane monolayer, containing free amino groups, through chemical reaction between its hydroxyl groups located on the surface of GO. This was followed by graft polymerization of acrylamide using redox system consisting of ceric ion and reducing groups (amino) on the surface of GO. This microwave assisted SI-RP offers a "greener" and much efficient method to synthesizing polyacrylamide-grafted-functionalized graphene oxide (FGO-PAM) nanocomposites. Since graphene is a derivative of graphite, thus graphene inherits its lubricating properties from graphite's solid lubricant behaviour. Polyacrylamide is also well established as aqueous lubricating additive in industry. Therefore, the application of FGO-PAM nanocomposites as aqueous lubricating additives has been investigated. Two of the important properties, coefficient of friction (COF) and wear reduction are investigated to establish the tribological efficiency of FGO-PAM composite.

Experimental

Materials

Graphite flakes and 3-aminopropyltriethoxysilane (APTES) were purchased from Sigma Aldrich. Potassium permanganate, sodium nitrate, concentrated sulphuric acid, 30% hydrogen peroxide, hydrochloric acid, ceric ammonium sulphate (CAS), acrylamide (AM) were purchased from MERCK India. All these chemical are of analytical grade.

Preparation of graphene oxide (GO)

GO was prepared from graphite flakes using modified Hummers method.[8] In a typical synthesis, concentrated H_2SO_4 (34 ml) was added into a flask containing Graphite flakes (1g) and Sodium nitrate (0.75g) under stirring at 0 ^oC (ice bath). Approx. 4.5 g $KMnO_4$ was added gently to the mixture over half an hour with the aid of stirring. The mixture was kept under stirring at room temperature for five days. Then, excess deionized water was added to the mixture. Finally, 30% H_2O_2 solution (2.7 ml) was added to complete the oxidation and the mixture resulted in a brilliant yellow colour with bubbling. The resultant mixture was rinsed with 5% HCl solution and washed with excess deionized water followed by sonication and centrifugation several times (minimum 5 times), filtered and vacuum dried.

Functionalization of GO with APTES

Dried GO powder (250 mg) was dispersed in toluene (100 ml) using ultrasonicator for 15 minute at room temperature. APTES coated GO nanosheets were achieved by refluxing the dispersed GO with 2 ml APTES in toluene under nitrogen protection for 24 h at 110 ^oC.[10] After the reaction was over, the resultant was carefully filtered through a PTFE membrane with a pore size of 0.2 µm, and washed with toluene at least three times to remove the residual APTES. The product (FGO) was dried overnight under vacuum at 60 ^oC.

Surface initiated-redox polymerization (SI-RP) of acrylamide under microwave irradiation

In a typical process, 25 mg of FGO was added in 50 ml of DI water, and then ultra-sonicated for 20 minutes to obtain a FGO dispersed solution. After adding acrylamide monomer (1 to 5 g) and de-aeration of the system by bubbling nitrogen for 30 minutes, 1.0 ml of 0.1 M solution of ceric ammonium sulfate (CAS) in 2N H_2SO_4 was added into the mixture to initiate the redox polymerization. The reaction was carried out under 700W microwave irradiation (MILESTONE microwave reactor) at 50 ^oC for 5 minute reaction time along with 5 minute ramping time. After the reaction FGO-PAM nanocomposite was obtained by precipitation, filtration, washing and drying overnight in a vacuum oven.

Characterization

Instrumental characterization

FT-IR spectra were recorded with a FTIR Spectrometer Nicolet 8700 FTIR spectrometer using a DTGS TEC detector in the region of 4000-400 cm^{-1}. The GO and nanocomposite were characterized with a Perkin Elmer lambda-19 UV-VIS spectrometer. The qualitatively spectra of GO and FGO-PAM nanocomposite were obtained for dilute aqueous solution. Raman Spectra of the samples were obtained using SPEX 1403 Raman spectrometer at 632 nm laser excitation. X-ray diffraction patterns were recorded using Cu Kα radiation (λ= 1.5406 Å) at 40 kV and 40 mA in the range of 2θ=2-60° with an XRD D8 advance Bruker diffractometer. Dried powder samples were mounted on the holder and proportional counter detector was set to collect data @1° min^{-1} with increment of 0.01° for 2θ values. Approx. 2-4 mg of samples was mounted on the sample holder for TGA analysis by Perkin Elmer TG/DTA diamond under N_2 atmosphere. The temperature range under study is 30-800 $^\circ$C with scan of 5 $^\circ$C per min. Scanning electron microscopy was conducted to analyse micro-structural changes on graphene oxide and nanocomposites samples. Prior to analysis by SEM the samples were dried using a vacuum drying oven at 45 $^\circ$C after which they were mounted on sample holders and coated with gold. SEM images of samples were taken by using FESEM, Quanta 200 F at a voltage of 10-30kV. TEM analysis was carried out on a FEI-Tecnai G^2 S-Twin TEM instrument operated at 200 kV.

Tribological characterization

The tribological tests of neat polyacrylamide and FGO-PAM nanocomposites were performed on a DUCOM, India make TR-30H four-ball test machine, in which a bearing ball is rotated in contact with three fixed balls, which are immersed in the aqueous sample. The upper rotating ball is held in a chuck at the lower end of a vertical spindle of a constant speed electric motor operating at a constant speed of 1200 rpm. The lower fixed balls are held

in position against each other in a steel cup by means of a clamping ring and locking nut. The cup assembly is supported above the load lever by a disk which rests on a thrust bearing thus allowing horizontal displacement and automatic alignment of the three lower balls against the upper ball.

The four ball geometry forms a tetrahedron making three contacts between top and bottom three balls. FGO-PAM composite as aqueous lubricant is filled in the cup such that the three balls are completely immersed in the sample. The load is applied through a loading lever and thus the contact is loaded. The resistive rotational torque acting on the spindle is continuously measured during torque sensor and converted into frictional force. Wear behaviour reported in terms of wear scar diameter (WSD) obtained on the balls and measured at the end of the tests by optical microscope. Properties of the lubricating additive were evaluated as per IP-239 test method. The samples were prepared at different loading of additives in aqueous solution. The test was conducted at 40 ^{0}C with sliding speed of 1200 rpm under a normal load of 20 Kgf (196 N) for one hour. The calculated COF and WSD are plotted by error bar with standard deviation of these values.

Results & Discussion

It has been reported that Ce (IV) ions in combination with organic reducing agents such as alcohols and amines act as redox pair thus functioning as an effective initiator for radical polymerization of a variety of aqueous vinyl monomers.[18, 28] In this paper we proposed a redox system consisting of ceric ion and reducing groups (amino) attached on the surface of GO sheets as initiator for the redox polymerization of acrylamide. A covalent linkage between PAM and functionalized GO sheets could be established by an efficient surface-initiated redox polymerization (As shown in Scheme 1).

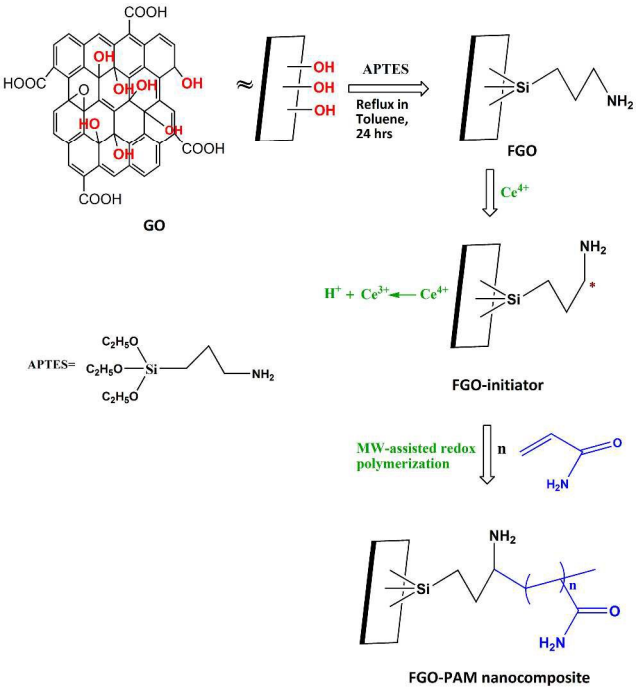

Scheme 1: Synthesis of FGO-PAM nanocomposite by microwave assisted surface-initiated redox polymerization

It has also been reported that Ce(IV) ions could participate in both initiation and termination steps of redox polymerization.[18,22] Therefore, Ce(IV) ion concentration plays a vital role in such redox polymerization. The effect of concentration of Ce(IV) ions on SI-RP are investigated with a concentration ranging from 0.122 x 10^{-3} to 3.92 x 10^{-3} M at a constant amount of FGO and monomer (Table S1). From the yield pattern of grafted polymer, 1.9 x 10^{-3} M of Ce(IV) ions concentration is found to be optimal for this polymerization system as this concentration gives highest yield.

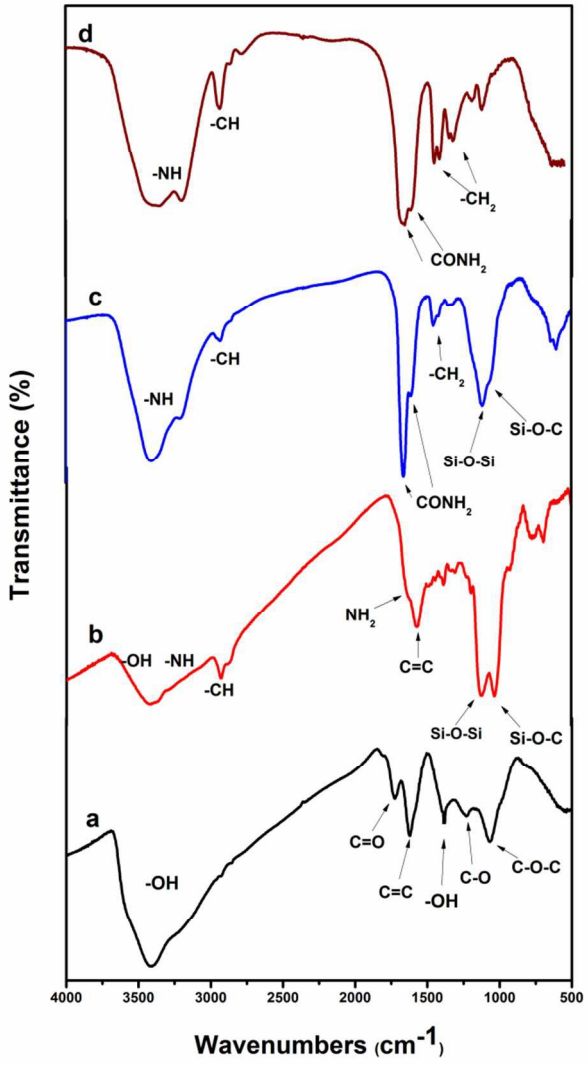

Fig. 1 FTIR spectra of (a) GO, (b) APTES functionalized GO (FGO) and (c) FGO-PAM nanocomposite (d) neat PAM.

The synthesized FGO-PAM nanocomposites (refer to scheme 1) are well characterized by different analytical techniques like FT-IR, UV-Vis, Raman, XRD, TGA, FE-SEM and HRTEM. The FTIR spectra of GO, APTES functionalized GO (FGO) and FGO-PAM nanocomposites are shown in Fig. 1. The formation of GO (Fig.1a) is clearly established from the characteristic peaks of GO at 3409 cm^{-1}(O-Hst), 1725 cm^{-1}(C=O st), 1622 cm^{-1} (C=C st), 1228 cm^{-1} (C-O st) and 1067 cm^{-1} (C-O-C). The presence of NH_2 group from 3390 cm^{-1} and 1645 cm^{-1} peaks (Fig. 1b) confirms the formation of FGO. The vibrational peak at 1566 cm^{-1}, 1122 cm^{-1}

and 1032 cm^{-1} are attributed to C=C, Si-O-Si and Si-O-C bonds respectively, indicating successful chemical bonding of APTES onto the surface of GO.[10] Moreover, the propyl chain is confirmed by peak at 2900 cm^{-1}. After polymerization, a new band is observed at 1660 cm^{-1} and 1611 cm^{-1} corresponding to the stretching and bending vibration of –C=O groups of the amide functionality of polymer chain. Broad bands at 3203 cm^{-1} and 2930 cm^{-1} are assigned to N-H and C-H stretching vibration of grafted polymer, respectively. The characteristic peak of silane at 1115 and 1050 cm^{-1} along with polymer chain are also observed in the FGO-PAM nanocomposite as compared to neat PAM (Fig 1d) which establishes the formation of grafted polymer brushes on the surface of APTES functionalized GO (refer Scheme 1). Formation of GO and FGO-PAM nanocomposite are further confirmed from UV-Vis spectra as shown in Fig. 2. In GO, the absorption at 234 nm corresponds to the π-π* transition of the aromatic followed by a shoulder at ~300 nm corresponding to the n-π* transition of the C=O bond. The nanocomposites retain the same UV characteristic feathers with little shift (253 nm and 325 nm).

In the Raman spectrum (Fig. 3), the characteristic D and G band for GO (Fig. 3a) are observed at 1319 cm^{-1} and 1586 cm^{-1}, respectively. The G band arises from the first order scattering of the E_2g phonon of sp^2 hybridized carbon and D band corresponds to the disordered, defect and edge oxy-carbons in graphene.[29] The D/G intensity ratio of GO in Raman spectra is found to be 1.06, which indicates the defects in graphene sheets, thus envisages here a lot of oxy functionalities present in graphene sheets. Thickness of aromatic sheets is calculated from intensity ratios of D and G bands using the equation E_L^4 (ID/IG) = $4300/L_d^2$.[30] Diameter of the aromatic sheets of the GO is found to be 16.67±5 nm at 632.8 nm (1.96 eV) laser excitation. In case of FGO-PAM nano-composite these D and G band are little shifted to 1324 cm^{-1} and 1595 cm^{-1} because of bonding of GO with polymer (Fig. 3b). The second order of D, called 2D band (overtone) and D+D' combination band are also observed at 2651 and 2900 cm^{-1}, respectively. The D/G ratio is changed from 1.06 (GO) to 1.15 (FGO-PAM) indicating higher degree of disorderness in graphitic lattice. This high D/G ratio of nanocomposite (FGO-PAM) is due to defects by covalently grafted polymer chains on the surface of FGO sheets.[13, 14]

The information about the lattice parameters such as inter-lamellar distance, layer diameter, and height of stacking layers, number of aromatic layers in GO and FGO-PAM are obtained from XRD spectra as shown in Table 1. There are two bands observed in XRD of GO (Fig. 4a). The sharp peak at 2θ value of 10.8^0 with 'd' value of 0.81 nm corresponds to 001 plane of exfoliated graphene oxide layers intercalated by water with interaction of oxy functional groups. Besides, a small but broad peak around 42^0 in GO corresponds to internal reflections of 10 and 11 planes within aromatic layer. The intercalated GO are stabilized with many oxy functionalities such as hydroxyl, epoxy, carboxyl groups etc., as evident from higher 'd' value (8.19 Å) than graphitic carbon (3.58 Å). The Bragg's relation was used in composite for calculating layer distance between aromatic sheets from the graphitic band (Fig. 4b). The average height of the stack of aromatic sheets, L_c, is calculated from the full width at half maximum of the graphitic band at 24.8^0 using the Scherrer's formula,[31, 32] L_c=0.9 λ/ωcosθ, where ω is the bandwidth. The average diameter of stacked aromatic sheets, L_a, is calculated by L_a=1.84 λ/ωcosθ. The number of aromatic sheets in a stacked cluster, M, is calculated from the values of L_c and d_m using M = (L_c/d_m)+1. The average height of stacked aromatic sheets is calculated for GO using the above formula and found to be 14 nm, whereas, the average height of stacked aromatic sheets calculated from Raman spectra of GO is 16.65 ±5 nm. The number of stacked aromatic layers is found to be 9 in GO. When GO is anchored with PAM, in XRD the GO band disappeared, instead a graphitic band appeared at 2θ of 24.8^0 with 'd' value of 3.58 Å. Therefore, the reaction of polymer with GO follows rearrangement of polymers along with shrinkage in aromatic sheet stacking whereby polymer chain packing happens at the edges. (Scheme 1). This further leads to semicrystalline nature of FGO-PAM as evident from the XRD peak pattern. Liu et al.[33] synthesized PAM hydrogel with superior ductility by in-situ polymerization of acrylamide in presence of GO. They observed GO acted as a cross-linker. With the presence of GO in the composite matrix a unique organic/inorganic network structure is formed between PAM chains and GO nano sheets through hydrogen bonding and physical adsorption. This finding is further substantiated by higher stacked layer of FGO-PAM than GO when calculated from XRD. Further, the number of stacked aromatic layer is also increased in composite. The number of aromatic layers increased from 9 to 67 is indication of aromatic sheets restacking due to polymer interaction with GO followed by rearrangement in FGO-PAM. This structural arrangement of higher stacked layers in FGO-PAM gives the advantage in enhancing tribological properties as discussed later.

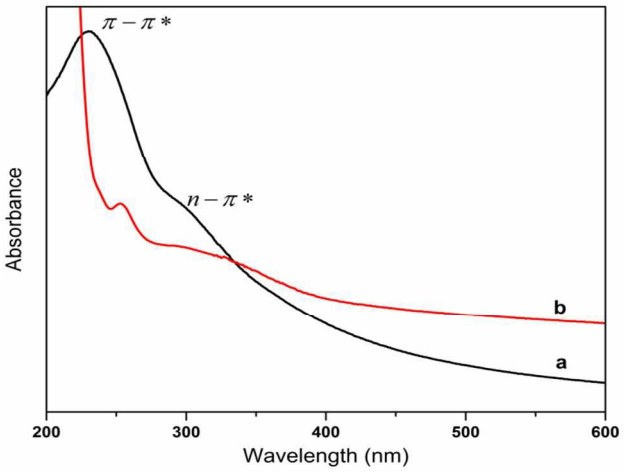

Fig .2 UV-Vis spectra of (a) GO and (b) FGO-PAM nanocomposite.

Table 1: XRD derived structural parameters of GO and FGO-PAM.

Parameters	*GO*	*FGO-PAM*
2θ (degree)	10.8	24.8
d (A^0)	8.19	3.587
FWHM (radian)	1.294	0.353
Average height of the stacked aromatic sheets L_c (A^0)	63.37	236.45
Average diameter of stacked aromatic sheets L_a (A^0)	129.55	483.42

No of aromatic sheets M	9	67

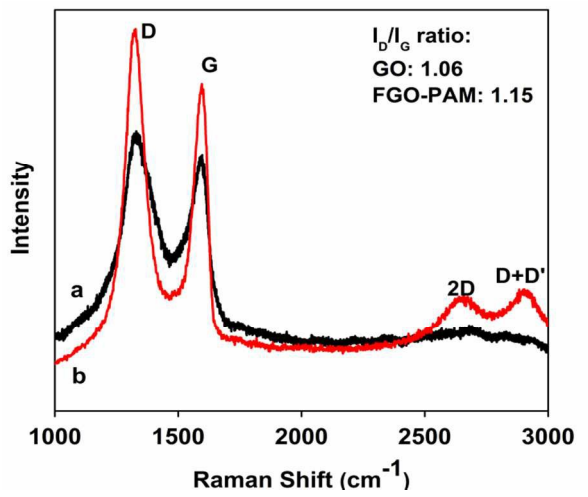

Fig. 3 Raman spectra of (a) GO and (b) FGO-PAM nanocomposite.

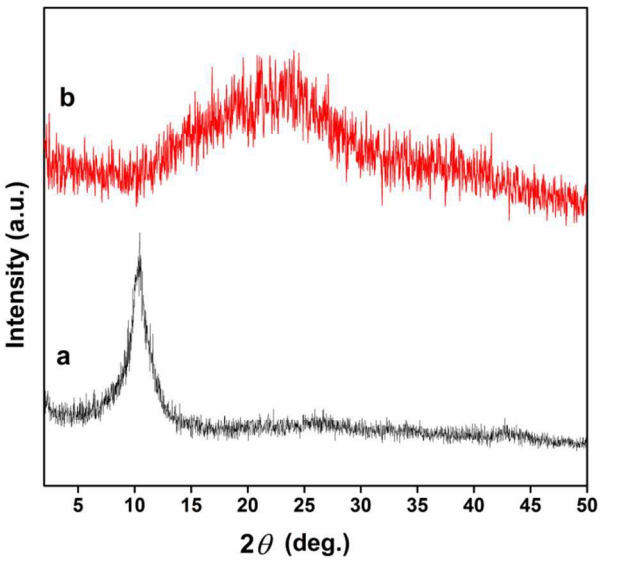

Fig. 4 XRD spectra of (a) GO, and (b) FGO-PAM nanocomposite.

Usually polymeric nanocomposites exhibit higher thermal stability compared to the corresponding polymer component. Therefore, TGA analysis was carried out not only to understand the thermal behaviour of the nanocomposites, but also to understand the thermal dependence of grafting density of polymer on FGO. Fig.5 displays TGA weight loss curves of GO, FGO and FGO-PAM nanocomposites.

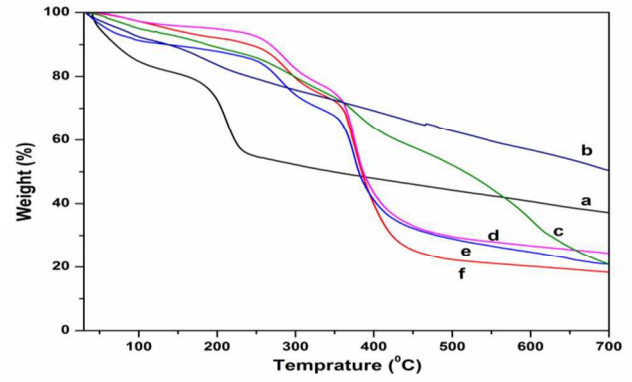

Fig. 5 TGA curves of (a) GO, (b) FGO, and (c, d, e and f) FGO-PAM nanocomposites with gradual increased grafted polymer contents.

The weight loss at 100 ^{0}C of GO is due to physically adsorbed molecules and the main weight loss of GO is found at 200 ^{0}C, attributed to the decomposition of labile oxygen-containing functional groups. Again, after the functionalization of GO with APTES (FGO) thermal stability is improved and the weight loss is reduced. In contrast to FGO, the TGA curves of nanocomposites show a major weight loss at a temperature around 350 ^{0}C corresponding to decomposition of polyacrylamide chains. Polyacrylamide usually displays thermal phase transition at around 175-200 ^{0}C (Tg), whereas, our nanocomposite (FGO-PAM) displays higher transition implying that the strongly anchored polyacrylamides increase the thermal stability. Furthermore, it is found that there is incremental weight loss with increase in polymer density in FGO-PAM (d, e and f compared to c in Fig. 5). TGA graph of nanocomposites also shows increased weight loss with increasing of polymer content (Fig. 5 c, d, e and f, respectively). By considering the weight loss at 250-500 ^{0}C due to polymer backbones and side chains in nanocomposites, it can be calculated that the grafting of polymer chains in nanocomposites increased from 35.34 % to 68.36 % that happens with increase of feeding amount of monomers.

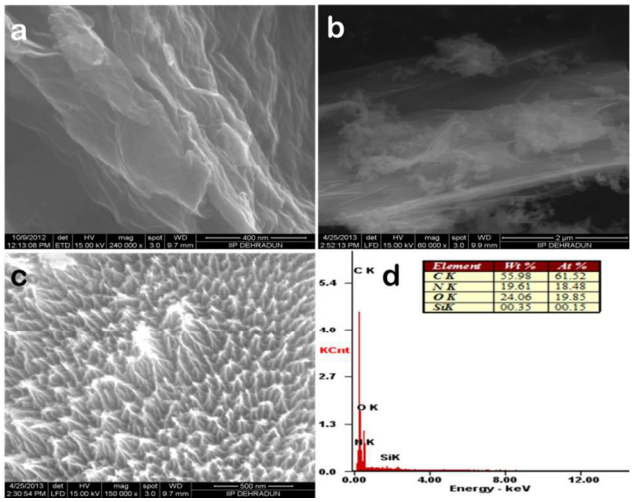

Fig. 6 SEM images of; (a) GO, (b) & (c) FGO-PAM nanocomposite at low(1g AM) and high (5 g AM) polymer content and (d) EDX of FGO-PAM composite..

The surface morphology of any composite can give

information about its tribological behaviour. Since we are interested to know about the two improved tribological properties such as COF and WSD of FGO-PAM, therefore, we investigated morphologies of GO and FGO-PAM nanocomposite by FE-SEM (Fig.6), and HRTEM (Fig. 7). Fig. 6a, SEM of GO, shows many stacked layers that are condensed and gives a look of bundle of many papery sheets. On the other hand, SEM image of FGO-PAM nanocomposite (Fig. 6b, c) shows different morphological structure at lower and high concentrations. At low concentration of polymer (Fig. 6b), a non-uniform polymer grafting is observed on the FGO sheets. These polymer structures are initiated from the surface of FGO using a redox couple with Ce (IV) ions. At high concentration of polymer, dense polymeric brushes are observed on FGO sheets (Fig. 6c).

TEM analysis (fig 7) of GO and FGO-PAM nanocomposites are employed for further substantiating the results. TEM image of GO (Fig 7a) shows flakes like shape where the edges tend to fold and roll. Fig 7b shows a higher magnification of GO where it clearly indicates the formation thin layers of GO sheets. TEM view of FGO-PAM nanocomposite (Fig 7c) shows some dark elongated bead like shapes on the nano-sheets while contrasting against GO image (Fig. 7a). These dark spots are due to the collapse structure of grafted polymer brushes onto the surface of FGO sheets as described with different polymer elsewhere.[13, 34]

Evaluation of Tribological properties of FGO-PAM

Friction and wear properties of FGO-PAM nanocomposites are evaluated at different loading of additive content as discussed in experimental section.

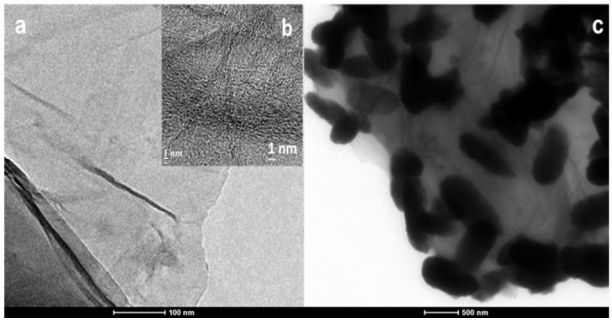

X

Fig.7 TEM images of; (a) GO, (b) at higher magnification of GO and (c) FGO-PAM nanocomposite.

Lubricating properties in terms of wear scar diameter (WSD) and coefficient of friction (COF) have been investigated for FGO-PAM nanocomposites with different loadings in aqueous medium by four ball tribo-machine and results are shown in Figure 8. The neat polyacrylamide is taken as a control experiment where COF is found to be around 0.16 and WSD calculated by optical microscope is 1.025 mm. The COF and WSD of FGO-PAM nanocomposites are found to be lower than neat polyacrylamide and a maximum reduction occurred with loading of 0.8 wt% FGO-PAM for both COF and WSD. The optimum loading (0.8 wt %) of FGO-PAM nanocomposites exhibited up to 37% increase in wear resistance and up to 55 % reduction in friction coefficient. Loading of nanocomposite beyond 0.8 wt % COF and WSD started increasing (Fig. 8(i and ii)). This inclined trend of COF and WSD at higher content of FGO-PAM beyond 0.8 wt%, may be due to agglomeration or non-dispersivity of FGO sheets after a certain compositional content (GO and polymer) in nanocomposite. It can be concluded that at an optimum concentration of FGO in nanocomposites, takes part in formation of uniform tribo film on the surface of steel balls is formed and further increase in content may disrupt the film surface.

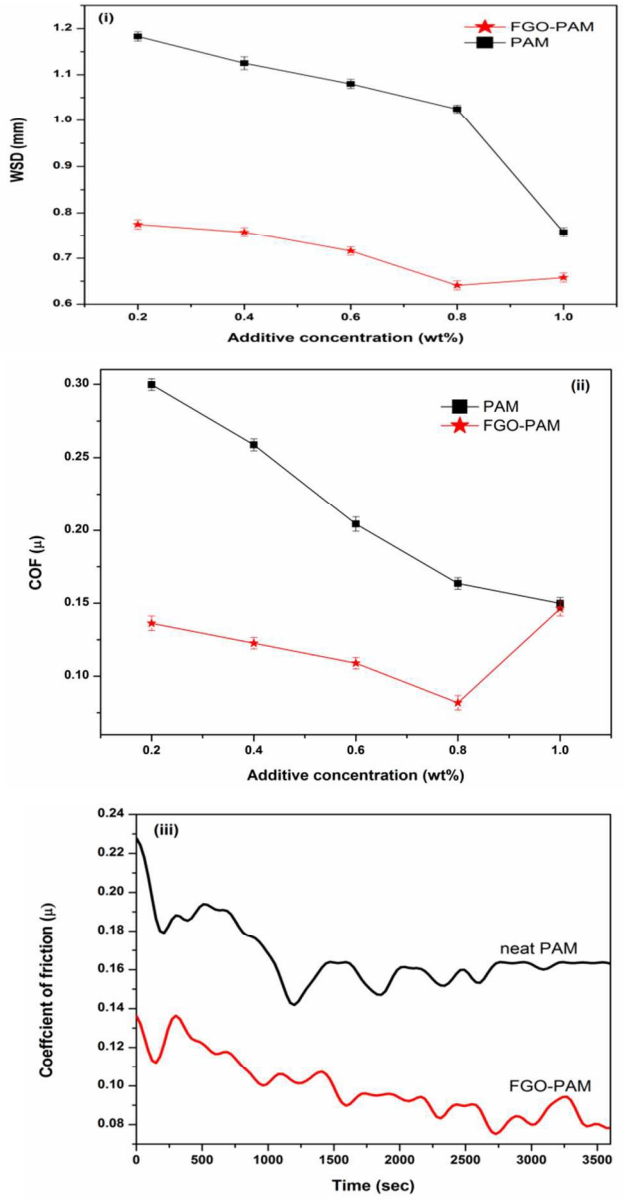

Fig. 8 (i) Friction and (ii) wear behaviour of FGO-PAM nanocomposites and neat PAM at different loading of additives; (iii) Comparison of COF pattern of FGO-PAM (0.8%) with neat PAM.

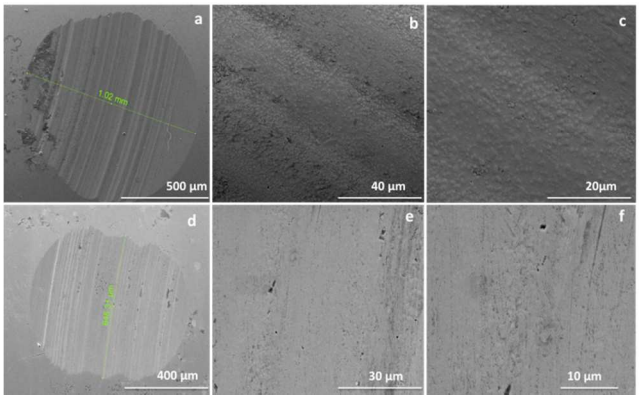

X

Fig. 9 FESEM images of worn surface of steel balls after tribo test: (a-c) neat PAM and (d-f) FGO-PAM nanocomposite at 0.8 wt % loading.

Wear behaviour was further examined from the morphology of the worn surface of steel ball through FESEM of ball surfaces collected after completion of tribo test of 60 min duration. SEM images of neat polyacrylamide Fig. 9(a-c) illustrate higher wear scar diameter with many scratches and debris. In contrast, nanocomposite forms uniform tribo film that reduces wear scar on the surface of steel balls Fig. 9(d-f). The tribo film prevents direct contact of the steel balls and therefore reduces friction and improves wear resistance. Thus, optimal quantity of FGO-PAM can be a better aqueous lubricating additive in improving of anti-friction and anti-wear properties.

Conclusions

A water soluble FGO-PAM nanocomposite prepared by microwave-assisted surface initiated redox polymerization provides a synthetic method that is rapid, green and efficient compared to conventional methods. The amine groups of functionalized GO are more approachable towards polymerisation in a redox couple with Ce(IV) ions. The grafting of polyacrylamide could be controlled and optimised with the Ce(IV) ion concentration and variation of monomer content. The nanocomposite demonstrates to be a potential aqueous lubricant additive with relatively better tribological properties in terms of better coefficient of friction reducer as well as enhanced wear resistance.

Acknowledgements

A. Kumar acknowledges UGC, Govt. of India for providing the financial support. Mr Raghuvir Singh, G.M. Bahuguna, Siya Ram, Sandeep Saran, K. L. N. Siva Kumar are acknowledged for recording spectra for FTIR, UV, XRD and SEM respectively. Finally the work is funded by CSIR under project OLP-0694 and DST, New Delhi under project GAP-5219.

Notes and references

* *CSIR-Indian Institute of Petroleum, Mohkampur, Dehradun, 248005, India. Fax: +91-135-2660202; Tel: +91-135-2525771; E-mail: ssray@iip.res.in*

† Electronic Supplementary Information (ESI) available: [Experimental detail of Table S1 and S2].

1. S. Stankovich, D. A. Dikin, G. H. B. Dommett, K. M. Kohlhaas, E. J. Zimney, E. A. Stach, R. D. Piner, S. T. Nguyen and R. S. Ruoff, *Nature*, 2006, **442**, 282–286.
2. H. J. Salavagione, G. Martínez and G. Ellis, *Macromol. Rapid Commun.,* 2011, **32**, 1771−1789.
3. D. R. Dreyer, S. Park, C. W. Bielawski and R. S. Ruoff, *Chem. Soc. Rev*., 2010, **39**, 228–240.
4. L. Kan, Z. Xu, and C. Gao, *Macromolecules*, 2011, **44**, 444–452.
5. J. Pyun, *Angew. Chem., Int. Ed*., 2011, **50**, 46-48.
6. J. Zhao, S. Pei, W. Ren, L. Gao, and H. M. Cheng, *ACS Nano*, 2010, **4**, 5245–5252.
7. H. Zhang, G. Gruner and Y. Zhao, *J. Mater. Chem. B*, 2013, **1**, 2542–2567.
8. W. S. Hummers and R. E. Offeman, *J Am Chem Soc*, 1958, **80**, 1339-1339.
9. Z. Liu, J. T. Robinson, X. Sun and H. Dai, *J. Am. Chem. Soc*., 2008, **130**, 10876-10877.
10. Y. Lin, J. Jin and M. Song, *J. Mater. Chem.,* 2011, **21**, 3455–3461.
11. Y. Cao, Z. Lai, J. Feng and P. Wu, *J. Mater. Chem.,* 2011, **21**, 9271–9278.
12. A. Badri, M. R. Whittaker and P. B. Zetterlund, *J. Polym. Sci. Part A: Polym.. Chem.*, 2012, **50**, 2981–2992.
13. M. Fang, K. Wang, H. Lu, Y. Yang and Steven Nutt, *J. Mater. Chem*., 2010, **20**, 1982–1992.
14. J. M. Bak and H. I. Lee, Polymer, 2012, **53**, 4955-4960.
15. P. Zhang, K. Jiang, C. Ye and Y. Zhao, *Chem. Commun*., 2011, **47**, 9504–9506.
16. Y. Deng, J. Z. Zhang, Y. Li, J. Hu, D. Yang and X. Huang, *J. Polym. Sci. Part A: Polym. Chem.,* 2012, **50**, 4451–4458.
17. A. Bansal, A. Kumar, P. Kumar, S. Bojja, A. K. Chaterjee, S. S. Ray and S. L. Jain, RSC Adv., 2015, **5**, 21189-21196.
18. A. S. Sarac, *Prog. Polym. Sci.,* 1999, **24**, 1149–1204.
19. Y. P. Wang, K. Yuan, Q. L. Li, L. P.Wang, S. J. Gu and X. W. Pei, *Materials Letters*, 2005, **59**, 1736–1740.
20. X. Pei, L. Hu, W. Liu and J. Hao, *European Polymer Journal,* 2008, **44**, 2458–2464.
21. B. Wang, D. Yang, J. Z. Zhang, C. Xi and J. Hu, *J. Phys. Chem. C*, 2011, **115**, 24636–24641.
22. L. Ma, X. Yang, L. Gao, M. Lu, C. Guo, Y. Li, Y. Tu and X. Zhu, *Carbon*, 2013, **53,** 269– 276.
23. Y. Mi, Z. Li, Z. Wang, J. Wang, X. Liu, S. Yang, H. Wang and J. Ou, *J. Mater. Chem*., 2012, **22**, 8036–8042.
24. J. Ou, J. Wang, S. Liu, B. Mu, J. Ren, H. Wang and S. Yang, *Langmuir,* 2010, **26**, 15830–15836.
25. H. Liu, Q. Wang, Y. Li and T. Wang, *J. Mater. Sci*, 2012, **47**, 1867–1874.
26. Y. Li, Q. Wang, G. Pan and T. Wang, *J. Mater. Sci,* 2012, **47**, 730–738.
27. S. A. Galema, *Chem. Soc. Rev*., 1997, **26**, 233-238.
28. K. Sui and L. Gu, *J. Appl. Polym. Sci.,* 2003, **89**, 1753–1759.
29. S. Stankovich, D. A. Dikin, R. D. Piner, K. A. Kohlhaas, A. Kleinhammes, A. Jia, Y. Wu, S. T. Nguyen and R. S. Ruoff, *Carbon*, 2007, **45**, 1558-1565.
30. L. G. Cancado, A. Jorio, E. H. M. Ferreira, F. Stavale, C. A. Achete, R. B. Capaz, M. V. O. Moutinho, A. Lombardo, T. S. Kulmala and A. C. Ferrari, *Nano Lett*., 2011, **11**, 3190-3196.
31. I. Schwager, P. A. Farmanian, J. T. Kwan, V. A. Weinberg and T. F. Yen, *Anal. Chem*., 1983, **55**, 42-45.
32. M. N. Siddiqui, M. F. Ali and J. Shirokoff, *Fuel,* 2002, **81**, 51-58.
33. R. Liu, S. Liang, X. Z. Tang, D. Yan, X. Li and Z. Z. Yu, *J. Mater. Chem*., 2012, **22**, 14160-14167.
34. G. Goncalves, P. A. A. P. Marques, A. Barros-Timmons, I. Bdkin, M. K. Singh, N. Emami and J. Gracio, *J. Mater. Chem*, 2010, **20**, 9927-9934.